AUTOMATYKA • 2010 • Tom 14 • Zeszyt 3/2

Krzysztof Grudzień*, Eric Maire**, Jerome Adrien**, Dominik Sankowski*

Analysis of Funnel Flow in Rectangular Silo Based on ECT Data

1. Introduction

About 60% of solid state industrial products appear, at some stage of production, as powders or grains. Many of them are stored in containers, majority in silos. The most popular shape type of silo is cylindrical, but very often rectangular silos are used, mainly in mining or construction industry. One of the characteristic points of the bulk solids flow are dynamic volume changes during processes of receptacle unloading. These changes depend on many factors, such as initial density of the granular material, stress level, mean grain diameter, specimen size and direction of the deformation rate. The difficulty lies in the determination of the time variant factors (humidity, temperature conditions, etc.) influence on the bulk solid storage behaviour. Usually it is not easy to forecast such dependences during design stage of the container. Monitoring of granular materials behaviour in silos is crucial for construction site safety. Therefore, accurate parametric description of shear localization zones in bulk solid is important, since in practice they inherently influence the wall stresses [8]. General and detailed studies with theoretical models for powder flow are reported by [5, 12].

The nature of powder systems makes them well suited for electrical capacitance tomography (ECT) investigation, since the measurement is based on differences in permittivity between electrically non-conducting powders and the surrounding medium [3, 4, 9, 11, 16, 17].

A variety of flow regimes can be observed within the silo itself according to the geometry and solid properties (Fig. 1). In case of silo flow can be distinguish two main types of flow [2, 4, 8, 11, 13]. The basic two types of flow behaviour are ‘mass flow’ and ‘core’ (or ‘funnel’) flow. Mass flow is characterized by all the material discharging uniformly with the same downward velocity across the entire cross section area, hence at a constant mass discharge rate. In contrast in ‘funnel’ or ‘core’ flow, as the name suggests, material is flowing

* Computer Engineering Departament, Technical University of Lodz, Poland
** Université de Lyon, INSA-Lyon, MATEIS CNRS, Villeurbanne, France

only in the centre of the hopper giving rise to stagnant zones of material at the walls of the container. There are number of inter-related parameters causing such undesired events to occur. These can be measured through assessment of factors affecting discharge time, for example: the angle of repose, porosity, bulk density, internal friction, packing density; hopper geometry, type of material (wall coefficient of friction) etc. Mass flow is preferred by the practitioners in industrial applications since it is stable and predictable, while the funnel flow causes problems with uniformity of flow and incomplete emptying of the silo. When the material tends to flow mainly in the core region of the container the rest of the solid situated close to walls is tending to form the so-called stagnant zones. Hence the material staying in these zones result in volume wastage and difficulties in process operation, for example uncertainty in amount and rate of material deployment into process installations. Therefore funnel type of flow regime is the target of investigation in order to measure and quantify these phenomena.

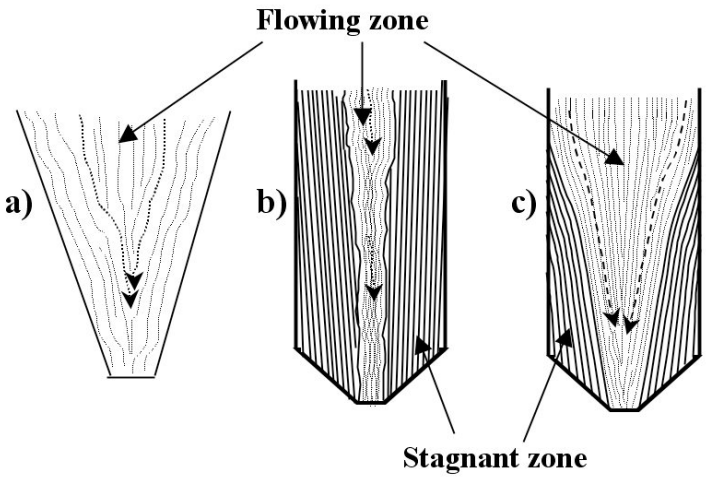

Fig. 1. Principal discharge hopper powder flow
(a – mass flow, b – funnel flow, c – semi-mass flow)

The innovations presented in the paper concern the applied ECT and X-ray tomography systems for analysis of sand concentration changes during discharging process of the rectangular funnel flow silo model. The previous works shown the application of ECT for monitoring sand concentration changes in cylindrical [2, 4, 8] and rectangular mass flow silo model's [9] during the silo discharging process. The funnel flow and mass flow are different regimes of gravitational flow in silo (Fig. 1). The different type of the flow regime demands different the ECT measurement sensors and as well different type of data analysis. In this paper are showing also results of the application X-ray 2D radiography and 3D tomography. Simultaneous measurements (ECT and X-ray tomography systems) conducted

during silo discharging process are additionally important part of innovations presenting in this paper.

The preliminary results presented in paper are the first step to determine ECT measurements error, comparing to the X–ray tomography measurements, and as well to understand better silo flow process. The obtained results (2D X-ray radiographs and 3D X-ray tomographs) are very helpful for better visualization and understanding the physics phenomena of the gravitational silo flow process.

2. Electrical Capacitance Tomography techniques

The main idea of the ECT technique is the production of an image of the cross-section area within a process vessel on the basis of measurements taken on its outer boundaries e.g. around the periphery of the process vessel or pipe [10, 16, 18] . The measured capacitances are related to dielectric constant of investigated materials or their permittivity. The relationship between capacitance on a pair of electrodes and permittivity is given by equation (1):

$$c = \frac{\oint_{\varsigma} \varepsilon(x, y) \nabla \varphi(x, y)}{V_c} \tag{1}$$

where:

V_c – the potential difference between the source and detecting electrodes,
$\varepsilon(x, y)$ – spatial permittivity at (x, y) coordinate,
$\varphi(x, y)$ – electric potential for (x, y),
ς – the curve bounding the electrode area in the cross-section plane.

Moreover the permittivity distribution is dependent on the density of material particles in the measurement space since the mixture of powder and air is considered in the case of solid material flow here. For the Maxwell models [8] the calculating of effective dielectric permittivity of a mixture is equation (2):

$$\varepsilon_{12} = \frac{\varepsilon_1 * (2\varepsilon_1 + \varepsilon_2 - 2 f_v(\varepsilon_1 - \varepsilon_2))}{2\varepsilon_1 + \varepsilon_2 + f_v(\varepsilon_1 - \varepsilon_2)} \tag{2}$$

where:

$\varepsilon_1, \varepsilon_2$ – the dielectric permittivity of the two components,
f_v – the volume fraction of material ε_2 in ε_1.

The relationship between the permittivity distribution and the capacitance measured between a pair of electrodes must be considered carefully in order to achieve accurate permittivity/concentration measurements. The careful solution of the mathematical relations

(where the ε is the unknown) governing the electrical field behaviour in the measurement field predicts, in effect, the permittivity distribution within the cross-section.

Application of ECT system for monitoring changes of material concentration insides sensor space is connected with two problems: inverse and forward problem [6, 15]. The mostly called of inverse problem is image reconstruction procedure. However before starting image reconstruction is necessary to conduct analysis of electrical field inside sensor space. Such analysis allows to prepare sensitivity matrix which is used for solve inverse problem in deterministic methods. Depends, what kind of methods is applied for visualised material distribution inside sensor, the sensitivity matrix can be calculate in each iteration algorithms step or only for beginning. The sensitivity matrix update for each iteration are answer to the nonlinear inverse problem for ECT imaging. The relationship between the electrical permittivity and measured capacitance is non-linear. The electrical field is disturbed by the material distribution, this phenomena is called "soft-field" effect.

The information about influence of the permittivity distribution changes inside vessel on measurement capacitance (between any pair of electrodes) is stored in sensitivity matrix. The form of this matrix is presented in equation (3):

$$S = \begin{bmatrix} s_{1,1} & s_{1,2} & \cdots & s_{1,L} \\ s_{2,1} & s_{2,2} & \cdots & s_{2,L} \\ \vdots & \vdots & \ddots & \vdots \\ s_{M,1} & s_{M,2} & \cdots & s_{M,L} \end{bmatrix}_{MxL} \tag{3}$$

where *i*-th element in *k*-th column contains knowledge about the magnitude impacts of dielectric constant changes in *i*-th pixels of tomographic image on the changes in *k*-th capacitance measurement.

The change in capacitance measured caused by an object located inside sensor varies with the position of the object relatively to the distance from electrodes. The electrical capacitance system is most sensitive in sensor area close to the walls of the vessel and is least sensitive at the centre zone of the vessel. There is a several ways to determine the sensitivity matrix. It can obtain as results of numerical calculation or by conducting measurement. The values of sensitivity matrix coefficients are dependent on the permittivity distribution inside sensor. This fact determines the nonlinear relationship between the capacitances measurements $\boldsymbol{C}$ and permittivity distribution ε. One with the most popular method for calculating the sensitivity matrix is based on Poisson equation [15]. It can be determine by solution to equation (4):

$$s_{kl,j} = -\int_{p(j)} \frac{E_{k,j}}{V_k} * \frac{E_{l,j}}{V_l} dj \tag{4}$$

where:

$E_{k,j}$, $E_{l,j}$ – means electrical fields inside j-th elements when one electrode – k, l is excited,
V_l, V_k – the voltage applied to individual electrodes,
$p(j)$ – j-th pixel.

In such way the sensitivity matrix $\boldsymbol{S}$ for the inverse problem is obtained [6, 15, 18]. The results of inverse problem solution is reconstructed image, which represents permittivity distribution in sensor space. To this end can be applied the Linear Back Projection method (LBP), which belong to the simplest image reconstruction methods, presented in equation (5):

$$\varepsilon = S^T * C \tag{5}$$

where:

ε – the normalized permittivity vector,
$\boldsymbol{S}^T$ – the transposed sensitivity matrix,
$\boldsymbol{C}$ – the normalized vector of the measured capacitances.

3. X-ray tomography techniques

The X-ray tomography system belongs to the "hard-field" tomography system. The path of measurements signal between source and detector is constant, it does not change under the influence of material distribution in measurements space (as took place for ECT tomography). X-ray radiation generated by source is going through object (in our case silo) and achieves detector. During this way radiation is attenuated by the object and number of photon on detector is smaller than emitted by source. The information about level of X-ray radiation attenuated allows to distinguish area of object with lower and higher density. The basic equation describing the attenuation of X-ray radiation determines Beer-Lambert law [1, 7], presented in equation (6):

$$N = N_0 \exp\left(- \int_{path} \mu(x, y)dx \right) \Rightarrow \ln \frac{N_0}{N} = \int_{path} \mu(x, y)dx \tag{6}$$

where:

N – number of photons transmitted single line trough investigated object,
N_0 – number of photons emitted by source,
$\mu(x, y)$ – value of linear attenuation coefficient in point (x, y).

It is necessary to remember that influence of material structure on X-ray radiation is connected with not only material density ρ but also atomic number Z and X-ray source

energy [1, 7, 14]. The linear absorption coefficient can be write in simply form based on equation (7):

$$\mu(E) = \rho * \left(F_1(E) + F_2(E) \frac{Z^{3.8}}{E^{3.2}} \right) \tag{7}$$

where:

F_1, F_2 – coefficient depends on the X-ray spectrum energy,
E – radiation energy,
Z – atomic number,
$\acute{N}$ – material density.

The details about X-ray radiation it can be find in [1, 7].

4. Experimental setup

4.1. Silo model

Experiments were conducted using the rectangular silo model stand made of Perspex. The model consisted of bin and hopper part (Fig. 2). The height of a mass flow silo was h = 0.29 m, the width b = 0.15 m, the depth d = 0.07 m. The width of the rectangular outlet along the silo depth was 5 mm. The wall thickness was 0.005 m. Such construction of silo model force symmetric funnel flow. During measurements was used smooth and very rough walls in a bin and a hopper sections (results presented in the paper are only for smooth wall). The silo has possibility of the outlet close during measurements (Fig. 2b). It was very helpful to visualise material distributions in form of 3D image during gravitational flow in case of X-ray tomography system application (Fig. 3). After several second free flow, the outlet can be close to stop the process and is possible to conduct rotations of silo for unchanging material distribution. It allows to investigate more accurate, based on 3D images, the gravitational flow of sand in silo. Figures 2 and 3 presents the project of silo and example photo from measurement campaign.

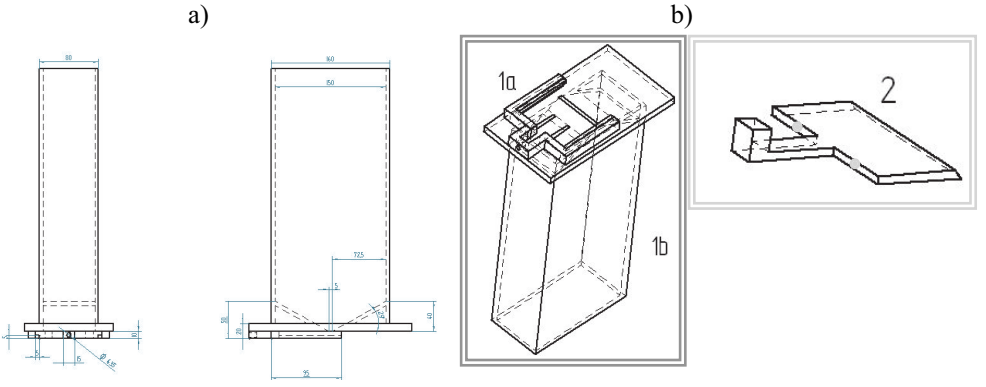

Fig. 2. Schema of silo model: a) main silo part; b) system for automatically close/open silo model

The tests were performed with a dry cohesionless sand with a mean grain diameter of d_{50} = 0.8 mm. An initially loose sand was obtained by filling the silo from a pipe located directly above the upper sand surface which was vertically lifted during filling. An initially dense sand was obtained by filling the silo using a so-called "rain method" (through a vertically movable sieve located always 250 mm above the upper sand surface in the symmetry-axis). The silo was emptied gravitationally.

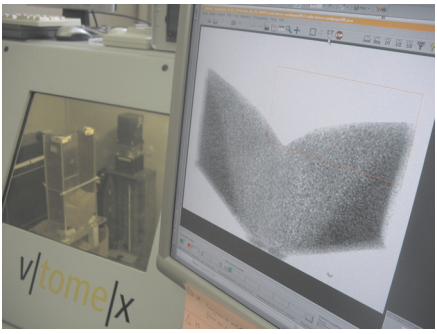

Fig. 3. On-line visualisation of the silo discharging process project by applied X-ray tomography system (X-ray system in Tomography laboratory INSA Lyon)

4.2. ECT sensor

In order to conduct measurements of sand concentration in silo flow was prepared 12 electrodes ECT sensor. The electrodes was located in pair on shorter side of silo and 4 electrodes on bigger side of silo. On Figure 4 is presented ECT electrodes system. The size of electrodes (16×3,3 cm) was dictated by size of silo – max distance between electrodes was about 15 cm. Signal to ratio of measurements signal had to be as small as possible.

a) b)

Fig. 4. ECT sensor: a) sensor located on silo wall; b) schema of electrodes layout

5. ECT measurements results analysis

The local solids concentration is associated with the measured permittivity of the mixed solids with air. The more dense packing the greater the value of permittivity in given region. Therefore, the change of packing density during discharging of silo conveys basic information describing the nature of discharge process. The dielectric permittivity distribution can be directly related to material concentration inside silo during discharging process. In this paper authors will be using term "concentration" instead of the normalised dielectric permittivity, which is connected to this.

On Figure 5 are presented the average changes of sand concentration during silo discharging process (taken directly from the measurements capacitance) in function of time for two different initially sand packing density (loose and dense). The most interesting part of silo discharging process is between 700 and 2500 frame number for initially loose packing density of sand and between 825 and 3250 for dense sand. The interpretation of average changes of sand concentration allows to conclude, that these changes are more noticeable for dense sand, where volume changes in sand characterizes more differential in sand packing densities for funnel area and area close to the wall silo. The changes (decreasing) of concentration for loose sand in funnel are reached about 3–5% initially level during stabilized flow. In case of dense sand this changes (increasing) is about 12–15%. The next different, between the sand behaviour for these two cases, is visible in silo discharging time, where in the case of dense sand time is longer for silo discharging.

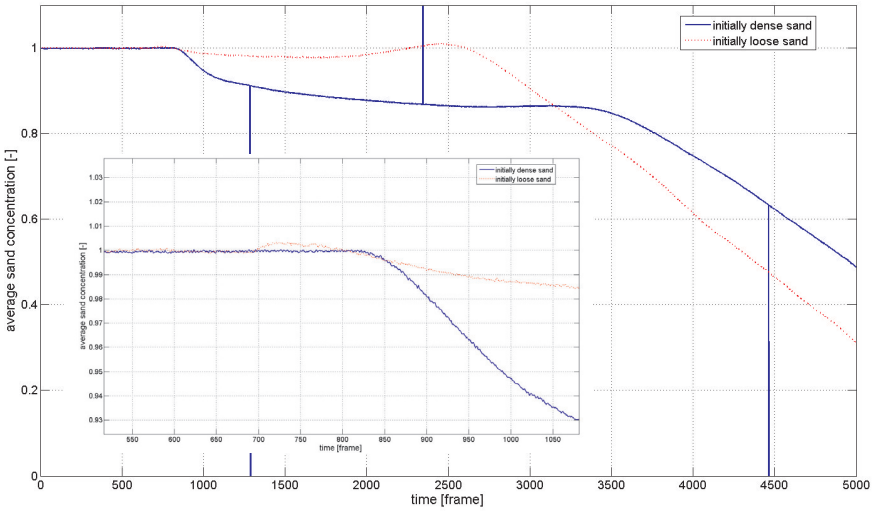

Fig. 5. Average sand concentration changes during gravitationally silo discharging process

In order to conduct more details analysis in terms of sand distribution ins sensor space is necessary to analyse the reconstructed images. On Figure 6 are presented images for two cases – loose and dense initially sand concentration – obtain for different stage of silo dis-

charging process. The reconstructed images are not very impressive. The part of capacitance measurements, especially for adjacent electrodes, was direct cause of error in image for area close to the silo wall. Applied LBP image reconstruction algorithm should be in future work replaced by more sophisticated methods. However the differences, which was visible on graph presented on Figure 5, are visible on images. The sand concentration in funnel area is lower for initially dens sand (≈ 0.75) comparing to initially loose sand (≈ 0.95). In order to estimate the wide of funnel area is necessary to conduct image processing and applied iterative image reconstruction methods.

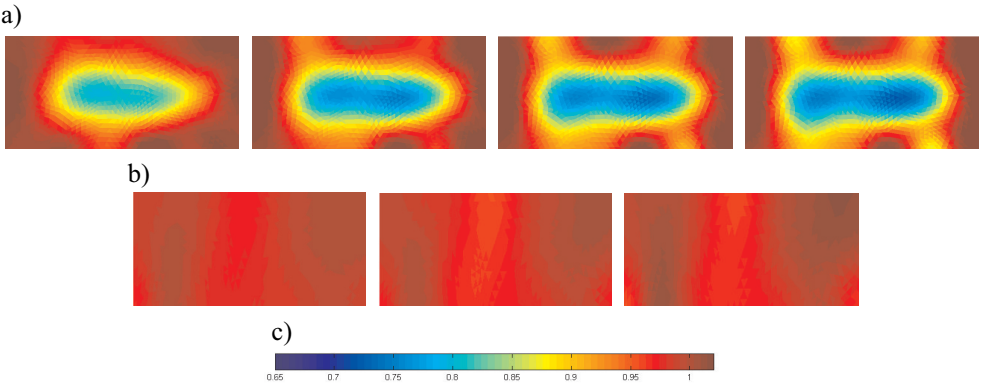

Fig. 6. Reconstructed images: a) initially dense sand for 1120, 1620, 2120 and 2620 frame number; b) initially loose sand for 1000, 1500, 2000 frame number; c) scale

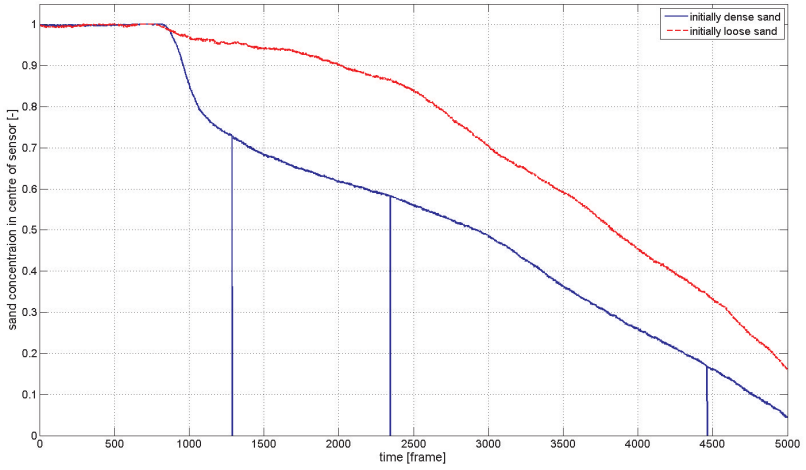

Fig. 7. Changes of sand concentration for dense and loose initially packing density of sand

Figure 7 shows plot of changes of sand concentration in funnel area (taken directly from the centre of reconstruction images). This graph more underlines the difference in sand concentration (in funnel area) between two cases of initially sand packing density.

In order to conduct validation of the ECT data analysis was applied X-ray system which allowed to visualize the silo discharging process in form of 2D radiographs.

6. X-ray system analysis

The presented results has concerned the application of X-ray tomography system to visualize the changes of solid concentration during the silo discharging process in form of radiographs and after to compare the results with the Electrical Capacitance Tomography measurements. Additionally the prepared system of the output/close silo outlet allowed to applied the 3D tomographs analysis methods to investigate movement of the particle tracers during the silos emptying. The measurements (ECT and X-ray) was conducted simultaneous. On Figure 8 is presented silo model in X-ray system with electrodes connected to ECT system.

Fig. 8. The simultaneous measurement of silo flow by ECT and X-ray tomography systems

Figures 9 and 10 present examples of sand distribution (for loose and dense sand) in silo with aid of 3D tomography, 2D radiography and 1D plot. Analysis of radiographs, especially 1D plot of intensity of X-ray on detector – cross the silo at 0.2 height, shows that

changes of sand concentration in case of loose sand are much smaller than for dense sand. Similar information, in terms of quality analysis, can be obtain based on ECT data. The quantity comparison between X-ray and ECT tomography systems requires a more detailed analysis of 3D tomography and 2D radiography in case of X-ray tomography system, similar as for ECT necessary is to applied better image reconstruction algorithms.

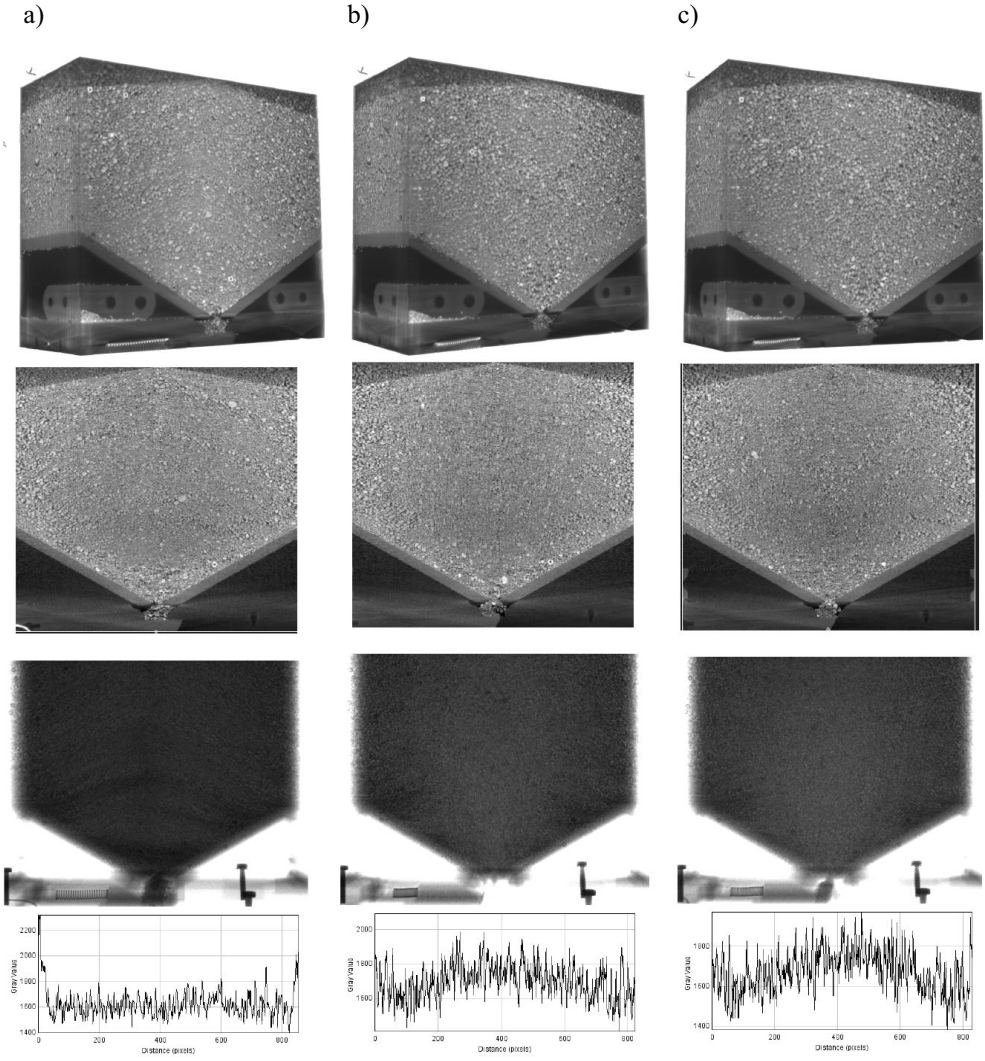

Fig. 9. Visualisation of sand concentration changes for loose sand – 3D tomography; 2D radiograph, 1D plot (cross the radiograph at height of silo 0.2): a) initial stage; b) after 8 s of flow (ECT frame number ≈1000); c) after 16 s of flow

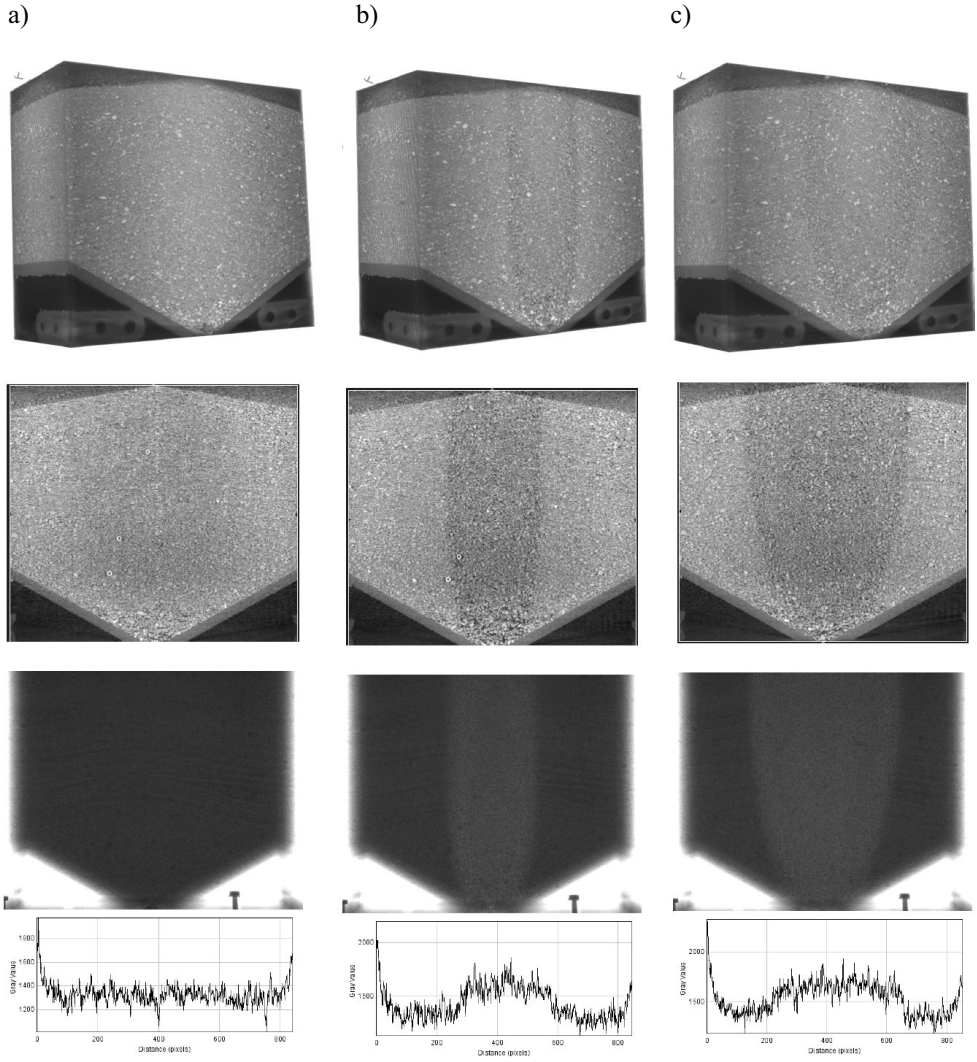

Fig. 10. Visualisation of sand concentration changes for dense sand – 3D tomography; 2D radiograph, 1D plot (cross the radiograph at height of silo 0.2): a) initial stage; b) after 8 s of flow (ECT frame number ≈1000); c) after 16 s of flow

7. Conclusion

Electrical Capacitance Tomography belongs to the non-invasive imaging of industrial processes. The main advantages of ECT system: robustness, fast, low cost comparing to the other tomographic methods, flexibility cause, that this techniques can be applied in moni-

toring and diagnosis industrial system. However in order to better interpret ECT measurement data and estimate error of ECT measurement necessary is to conduct validations procedure. The validation procedure using static phantoms is not the best solution for determine ECT tomography error, especially for industry applications. The presented researches show first step in order to verify ECT techniques compared to X-ray radiographs results. The obtained simultaneous measurements for silo discharging process using X-ray and ECT tomography systems allow to conduct the quantity comparisons between these two visualise techniques. Such comparison should give knowledge about accuracy of ECT tomography systems. In order to receive information about error of ECT measurements necessary is to conduct quantitative analysis of X-ray data, similar as presented in this paper in case of ECT data analysis.

The data analysis presented in paper, based on analysis sand concentration changes during silo flow, allow to conduct only the quality comparison between X-ray and ECT tomography systems. The results in both case of tomography systems show decreasing of sand concentration in funnel area comparing to the initial stage. However in case of X-ray system the sand concentration decreased is constant during silo flow and only size of funnel is changing (area of funnel is increasing in function of time). In case of ECT tomography decreasing of the sand concentration in funnel area displays continuous character (concentration is decreasing in function of time). Such results (this different between X-ray and ECT data) can be caused by increasing funnel area and influence this phenomena on ECT image reconstruction. This fact will be investigated in the future work of data analysis work.

Acknowledgments

The work is funded by the European Community's Sixth Framework Programme – Marie Curie Transfer of Knowledge Action (DENIDIA, contract No.: MTKD-CT-2006-039546). The work reflects only the author's views and the European Community is not liable for any use that may be made of the information contained therein.

K. Grudzien is a scholarship holder of project entitled „Innovative education" supported by European Social Fund.

References

[1] Baruchel J., Buffiere J.-Y., Cloetens P., Maire E., Merle P., Peix G., *X-Ray Tomography in Material Science*. Hermes Science Publications, Paris, 2000, 205.

[2] Chaniecki Z., Dyakowski T., Niedostatkiewicz M., Sankowski D., *Application of electrical capacitance tomography for bulk solids flow analysis in silos*. Particle and Particle Systems Characterization, 23, 3–4, 2006, 306–312.

[3] Dyakowski T., Edwards R.B., Xie C.G., Williams R.A., *Application of Capacitance Tomography to Gas-Flow Solids*. Chem. Eng. Sci., 52, 13, 1997, 2099–2110.

[4] Grudzien K., Romanowski A., Williams R.A., *Application of a Bayesian approach to the tomographic analysis of hopper flow*. Particle & Particle Systems Characterization, vol. 22, Issue 4, 2005, 246–253.
[5] Jenike A.W., *Storage and Flow of Solids*. Eng. Exp. Station Bulletin, 123 (University of Utah), 1970.
[6] Loser T., Wajman R., Mewes D., *Electrical capacitance tomography: image reconstruction along electrical field lines*. Meas. Sci. Technol., vol. 12, 2001, 1083–1091.
[7] Maire E., Adrien J., Carmena V., Buffičre J-Y., Courbon J., *In situ experiments in X ray tomography using synchrotron and standard laboratory tomographs*. 5th International Symposium on Process Tomography in Poland, Zakopane, 2008.
[8] Niedostatkiewicz M., Tejchman J., Chaniecki Z., Grudzień K., *Determination of bulk solid concentration changes during granular flow in a model silo with ECT sensors*. Chemical Engineering Science, vol. 64, Issue 1, 2009, 20–30.
[9] Niedostatkiewicz M., Tejchman J., Grudzień K., Chaniecki Z., *Application of ECT to solid concentration measurements during granular flow in a rectangular model silo*. Chemical Engineering Research and Design, vol. 88, Issue 8, August 2010, 1037–1048.
[10] Plaskowski A, Beck M. S., Thorn R. And Dyakowski T., *Imaging Industrial Flows, Institute of Physics Publishing*. Bristol, 1995.
[11] Romanowski A., Grudzien K., Williams R.A., *Analysis and Interpretation of Hopper Flow Behaviour Using Electrical Capacitance Tomography*. Particle & Particle Systems Characterization, vol. 23, Issue 3–4, 2006, 297–305.
[12] Seville J., Tuzun U., Clift R., *Processing of Particulate Solids*. Blackie Academic, London, 1997, 1997, 377.
[13] Słomiński C., Niedostatkiewicz M., Tejchman J., *Application of particle image velocimetry (PIV) for deformation measurement during granular silo flow*. Powder Technology, 173, 1, 2007, 1–18.
[14] Stock SR., *Recent advances in X-ray microtomography applied to material*. International Materials Reviews, vol. 53, No. 3, 2008, 129–181.
[15] Wajman R., *Nowa metoda rekonstrukcji obrazów dla potrzeb pojemnościowej tomografii procesowej*. Rozprawa doktorska, Politechnika Łódzka, 2006.
[16] Williams R.A., Beck M.S., *Process Tomography – Principles, Techniques and Applications*. Butterworth-Heinemann, Oxford, 1996, 507.
[17] Yang WQ., Liu S., *Electrical capacitance tomography with a square sensor*. 1st World Congress on Industrial Process Tomography, Buxton, 1999, 313–317.
[18] Yang WQ., Spink_D.M., Gamio_J.C., Beck_M.S., *Sensitivity distributions of capacitance tomography sensors with parallel field excitation*. Meas. Sci. Techn., vol. 8, 1997, 562–569.